Angewandte Chemie
Eine Zeitschrift der Gesellschaft Deutscher Chemiker

Supporting Information

Structure of Human Tyrosinase Related Protein 1 Reveals a Binuclear Zinc Active Site Important for Melanogenesis

Xuelei Lai, Harry J. Wichers, Montserrat Soler-Lopez, and Bauke W. Dijkstra**

anie_201704616_sm_miscellaneous_information.pdf

Author Contributions

X.L. Investigation: Lead; Methodology: Lead; Validation: Lead; Writing—original draft: Lead
H.W. Conceptualization: Equal; Supervision: Supporting; Writing—review & editing: Equal
M.S. Conceptualization: Equal; Methodology: Equal; Supervision: Lead; Validation: Equal; Visualization: Lead; Writing—review & editing: Equal
B.D. Conceptualization: Lead; Funding acquisition: Lead; Supervision: Equal; Writing—review & editing: Equal.

TABLE OF CONTENTS

Methods

Construct design and generation of recombinant baculovirus

The intramelanosomal domain (residues 25-471) of human TYRP1 (P17643, Uniprot), a truncated version of the full-length protein without the single-transmembrane domain and the cytosolic tail was chosen for our crystallographic study. The TYRP1 native N-terminal signal peptide (residues 1-24) was included in the construct to facilitate the secretion of the protein for post-translational modifications (such as glycosylation) in insect cell expression systems. Thus, a codon-optimized gene encoding the TYRP1 signal peptide and the intra-melanosomal domain followed by a Tobacco Etch Virus (TEV) cleavage site (ENLYFQG) and a hexa-histidine tag was commercially synthesized and inserted into pACEBac1 vector (Geneva Biotech) between *SacI* and *XbaI* restriction cloning sites. The resulting plasmid was confirmed by DNA sequencing (Macrogen Inc.) and subsequently transformed into DH10BacY bacterial competent cells for the production of recombinant bacmids. The cells were incubated in Luria-Bertani (LB) medium overnight at 310 K and subsequently plated on an agar plate containing kanamycin (50 µL/mL), gentamycin (10 µL/mL), tetracycline (10 µL/mL), isopropyl-β-D-1-thiogalactopyranoside (IPTG, 1 mM) and Bluo-Gal (100 µL/mL, Thermo Fisher Scientific Inc.) for blue-white screening to identify colonies containing the recombinant bacmid. A single white colony containing recombinant bacmids was picked and inoculated into 2 mL medium for bacmid extraction and purification. Purified DNA product was then mixed with DNA transfection reagent (X-tremeGENE HP, Roche) and used to transfect 3 mL of a culture containing one million *Sf21* insect cells (Thermo Fisher Scientific), according to manufacturer's protocol. Recombinant baculoviruses in the supernatant were harvested after 72 h incubation and used to subsequently infect 25 mL of *Sf21* cell culture (at a density of ~0.7 million cells per mL). High *multiplicity of infection* virus stocks were harvested after around 108 h and stored at 277 K for long-term use.

The full-length TYRP1 nucleotide sequence used in this study was codon-optimized for overexpression in insect cells, and synthesized by Shanghai ShineGene Molecular Biotech,Inc:

atgaagtttctggtaaatgtcgctttggtgttcatggtggtctacattagttacatctacgctcatcaccatcatcatcacgagaatttgtacttccagggtcagtttccacgtcagt
gtgcaacagtagaggcactccgctccggaatgtgctgccccgacctctctccggtgagtggaccaggcaccgatcgctgtggttcctcctcaggtcgcggtcgctgtgag
gcggtcactgctgatagtcgtccgcacagcccccagtatcctcacgacggacgtgacgatcgtgaagtgtggcctctgcgcttcttcaatcgcacctgccattgtaatggaa
acttttccggccataactgcggcacatgtcgcccaggttggaggggcgctgcctgcgatcaacgtgtgctcattgtaagacgcaatctgttggatctgagtaaggaggaga
agaaccacttcgtccgcgcactcgatatggcgaaacgtaccacccatccactcttcgtgattgccacgaggcgttctgaagaaatcctgggtcctgatggaaacacccct
caatttgagaacatatccatctacaactactttgtctggacacattattactccgtgaagaaaactttcctcggtgtgggccaggaaagctttggagaagtcgatttcagccac
gaaggacccgcattcttgacctggcaccgttaccatctgttgcgcctggagaaagacatgcaagaaatgctccaggagccgtctttcagtctcccgtactggaactttgcg
acaggtaagaatgtttgtgatatttgtactgatgatctgatgggtagtcgttcaaatttcgattccacactgatttctccaaactccgtttttttctcaatggcgtgtggtctgcgattct
ctcgaagactatgataccctgggtacactctgtaattcaacggaagatggtccgatcaggagaaaccccgctggaaatgtggcccgcccaatggttcagcgtctgccag
aaccacaggatgttgcccaatgcttggaagtgggcttgtttgataccccccctttctattccaattcaacaaactcattccgcaatacggtggagggatactccgacccgac
aggtaagtacgatcctgcggtaaggagcctgcataacctggcacacctttttcttgaacggtacgggaggtcaaacgcacctgagccctaacgatccgattttcgttctgctc
cacaccttcaccgacgccgtttttgatgaatggcttcgtaggtacaatgctgacatatcgacctttcctctggaaaacgccccgatcggccacaaccgtcaatacaacatgg
tccccttctggccgccggtgacaaacaccgaaatgtttgttactgcgccagacaacttgggttacacctacgaaattcaatggccgtcacgcgagttcagcgtacctgaga
taatcgcgattgctgtagttggtgctctccttctcgtggccctcatcttcggtactgcctcgtacctgatcagagccaggaggtccatggatgaggccaatcagcctctgttgac
agaccagtaccagtgctatgctgaggagtatgagaaattgcagaaccctaaccagtcggtcgtg.

Protein expression and purification

For large-scale expression, 4 mL recombinant baculovirus stock solution was used to infect 4 liters of *Sf21* cells (at a density of ~1.0 million cells per mL). After culturing for ~108 h, the medium was clarified by centrifugation at 6000 g and subsequently concentrated to ~100 mL using a 10 kDa cut-off QuixStand Benchtop System (GE Healthcare). The concentrated medium was then incubated with 5 mL of Ni-NTA agarose resin (QIAGEN) for 20 min, which was then applied to a 20 mL gravity flow chromatography column (Econo-Pac column, Bio-Rad). The flow-through was discarded

and the bound protein was washed with 2 column volumes (CV) of wash buffer (25 mM Tris-HCl, pH 7.8, 150 mM NaCl, 50 mM imidazole) and eluted with 1 CV of elution buffer (25 mM Tris-HCl, pH 7.8, 150 mM NaCl, 500 mM imidazole). TEV protease was added to the eluted protein solution and dialyzed overnight at 273 K against dialysis buffer (25 mM Tris-HCl, pH 7.8, and 150 mM NaCl) to cleave the C-terminal 6xHis-tag. TEV protease and uncleaved protein were removed by nickel affinity chromatography. Cleaved human TYRP1 protein in the flow-through was collected and buffer-exchanged to ion-exchange buffer (25 mM Tris-HCl, pH 8.8, 50 mM NaCl). The resulting protein solution was then applied to a MonoQ column (GE Healthcare) pre-equilibrated with the ion-exchange buffer. The flow-through fractions with pure TYRP1 protein were pooled, concentrated and applied to a final gel filtration chromatography column (Superdex-200; GE Healthcare) pre-equilibrated with crystallization buffer (10 mM Tris-HCl, pH 7.8, 100 mM NaCl). The elution fractions containing the pure protein were finally pooled and concentrated over a 30 kDa cut-off Amicon membrane (Millipore) to ~25 mg/mL for crystallization screening. Recombinant expression, purification and crystallization of human TYR intra-melanosomal domain (residues 19-456) have been reported elsewhere.[1] Insert cells were cultured using Sf-900™ III SFM (Thermo Fisher Scientific) medium without any supplementation.

Crystallization

Initial screening for crystallization conditions was performed by the HTX crystallization facility (EMBL-Grenoble, France). The crystallization screens were set up by sitting-drop vapor-diffusion using three protein and reservoir ratios (3:1, 1:1 and 1:3). All crystallization trials were done at 293 K. Crystals appeared in a condition containing 0.1 M Tris (pH 7.0), 0.2 M NaCl and 30% (w/v) PEG 3000, with a protein to reservoir ratio of 3:1. This condition was manually optimized by mixing 1.5 µl protein solution with 0.5 µl reservoir solution, and varying the pH and PEG 3000 concentration. Rod-like crystals appeared in 2 days and grew to full size in 7 days. Tyrosine was introduced in the crystals by soaking them with tyrosine powder, directly added and incubated overnight before harvesting for diffraction tests. Soaking of tropolone, kojic acid or mimosine was carried out by crystal soaking in a cryo-drop (reservoir solution supplemented with 20% (v/v) glycerol) containing the corresponding powder for 5 to 10 min before harvesting for diffraction tests. TYRP1-3M native and ligand-bound crystals were crystallized and prepared following a similar protocol as that of native TYRP1.

Data collection and processing

Crystals were mounted in cryo loops and subsequently flash-frozen in liquid nitrogen. X-ray diffraction data for native and ligand-bound TYRP1 crystals were collected at 100 K at beamlines ID23-1 or ID29 (European Synchrotron Radiation Facility (ESRF), Grenoble, France) (Table S1). Ligand-bound TYRP1-3M crystals were collected at the ESRF MASSIF-1 automated beamline.[2] Native crystals diffracted up to 2.3 Å, ligand-bound TYRP1/TYRP1-3M crystals diffracted between 2.5 and 2.8 Å. The data sets were processed and integrated using the program XDS[3] in combination with the program SCALA[4] from the CCP4 package.[5] The crystals belong to space group $P2_12_12_1$. For phasing native TYRP1, a modified model of tyrosinase from *Bacillus megaterium* (PDB: 3NM8)[6] was generated with CHAINSAW[7] by pruning non-conserved residues. Molecular replacement was carried out with PHASER[8]. The resulting single solution gave four molecules in the asymmetric unit, with each molecule displaying clear electron density for residues 126 to 467. Clear difference density was present for residues 25-125, which were not present in the search model. Further manual model rebuilding and refinement were iteratively performed with COOT and PHENIX,[9] respectively. The missing residues were subsequently added manually in COOT.[10] Ligand bound TYRP1/TYRP1-3M structures were solved by molecular replacement using native TYRP1 as a search model. Statistics of data collection and refinement are summarized in Table S1.

To confirm the presence of zinc ions in the native TYRP1 crystal, a single-wavelength anomalous dispersion (SAD) experiment was carried out on a single crystal. The SAD data was measured at beamline ID23-1 (ESRF, Grenoble) at the zinc *K*-edge (9.67 keV) (Table S1). The data set was processed and integrated using the program XDS[3] from the CCP4 package.[5] The native and the anomalous data sets were then merged with the program CAD to generate an anomalous difference Fourier map using the zinc anomalous signal with the program FFT from the CCP4 package.[5]

X-ray fluorescence data collection and processing

X-ray fluorescence data were collected at ESRF beamline ID23-1 with an incident beam energy of 12.7 keV, an exposure time of 1 s and a transmitted beam intensity of 2.2%.[11] Analysis of the X-ray fluorescence spectrum was handled by *PyMCA* (Python multichannel analyzer)[12] integrated in *mxCuBE.*[13]

Activity measurements

Tyrosine hydroxylase and L-DOPA oxidase activities were measured at 298 K using L-tyrosine and L-DOPA as substrates, respectively.[14,15] 90 µL pre-reaction mix containing 5 mM 3-methyl-2-benzothiazolinone hydrazone hydrochloride hydrate (MBTH), 125 mM potassium phosphate buffer, pH 6.8, 2.5% dimethylformamide (DMF) and saturated L-tyrosine/L-DOPA in a 10 mm-path cuvette was placed in a UV-visible spectrophotometer (UV-2401PC mode, Shimadzu Corporation). The reaction was started by addition of 10 µL protein solution to the pre-reaction mix, and was monitored by measuring the absorbance increase at 507 nm wavelength (ε_{507}=38000 M^{-1} cm^{-1}) in 5 or 10 min. DHICA oxidase activity was determined using DHICA (5,6-dihydroxyindole-2-carboxylic acid) as substrate in the pre-reaction mix.[16] The reaction was monitored by measuring the absorbance increase at 470 nm wavelength (ε_{470}=15000 M^{-1} cm^{-1}) in 5 or 10 min. The metal depleted protein samples (apo TYRP1, apo TYRP1-3M and apo TYR) were prepared by incubating the corresponding native protein sample with 100 mM KCN in Tris buffer, pH 7.5 at 4 °C overnight according to Martinez-Esparza et al..[17] The metal-substituted protein samples (TYR-Zn, TYRP1-Cu and TYRP1-3M-Cu) were prepared by incubating the corresponding apo protein sample with 0.5 mM $ZnCl_2$ or $CuCl_2$ in 50 mM Tris buffer, pH 7.5 at room temperature for 3 hours. All protein samples were buffer-exchanged to zinc- and copper-free buffer (50 mM Tris buffer, pH 7.5, 150 mM NaCl) before assays. All measurements were performed in duplicate or triplicate. A list of recombinant human tyrosinase activities reported in previous studies is shown in Table S2.

The on-plate tyrosinase activity was measured at 298 K using L-tyrosine as substrate in a Nunc™ Edge 96-Well plate (Thermo Fisher Scientific). Each well contained 100 µl pre-reaction mix, containing 4 mM MBTH, 100 mM potassium phosphate buffer, pH 6.8, 2% DMF and 1 mM tyrosine. The colorimetric reaction was started with the addition of 10 µL of protein solution to the pre-reaction mix, and was followed by monitoring the development of the pink coloured quinone-MBTH adduct. Reactions that showed tyrosinase activity in pre-tests (data not shown) were supplemented with tyrosinase inhibitors (wells 2*, 4* and 6*, respectively, Figure 4D), 5 mM tropolone and 1 mM phenylthiourea, in order to show specific tyrosinase activity. Protein samples used in the colorimetric reactions were concentrated to ~0.5 mg/ml for TYR, and ~5 mg/ml for TYRP1, TYRP1-Cu, TYRP1-3M and TYRP1-3M-Cu respectively. Images were taken using a Photo HP Scanjet G3110 scanner (Hewlett-Packard) after 0, 1 min, 10 min, 20 min, 40 min, 80 min and 160 min, respectively.

Site-directed mutagenesis

TYRP1-3M (Y362F-R374S-T391V) was generated by overlapping PCR using Phusion DNA polymerase (New England BioLabs). The primers were designed by PrimerX (www.bioinformatics.org/primerx/) and synthesized by Eurofins Genomics. The triple construct was generated stepwise in the order of Y362F, R374S and T391V. All mutant constructs were confirmed by DNA sequencing (Macrogen Inc.).

Accession codes

Coordinates and structure factors have been deposited in the Protein Data Bank under accession codes PDB 5M8L (native TYRP1), PDB 5M8P (TYRP1-tyrosine), PDB 5M8O (TYRP1-tropolone), PDB 5M8N (TYRP1-mimosine), PDB 5M8M (TYRP1-kojic acid), PDB 5M8R (TYRP1-3M-mimosine), PDB 5M8T (TYRP1-3M-tropolone), and PDB 5M8Q (TYRP1-3M-kojic acid).

Supplementary Figures

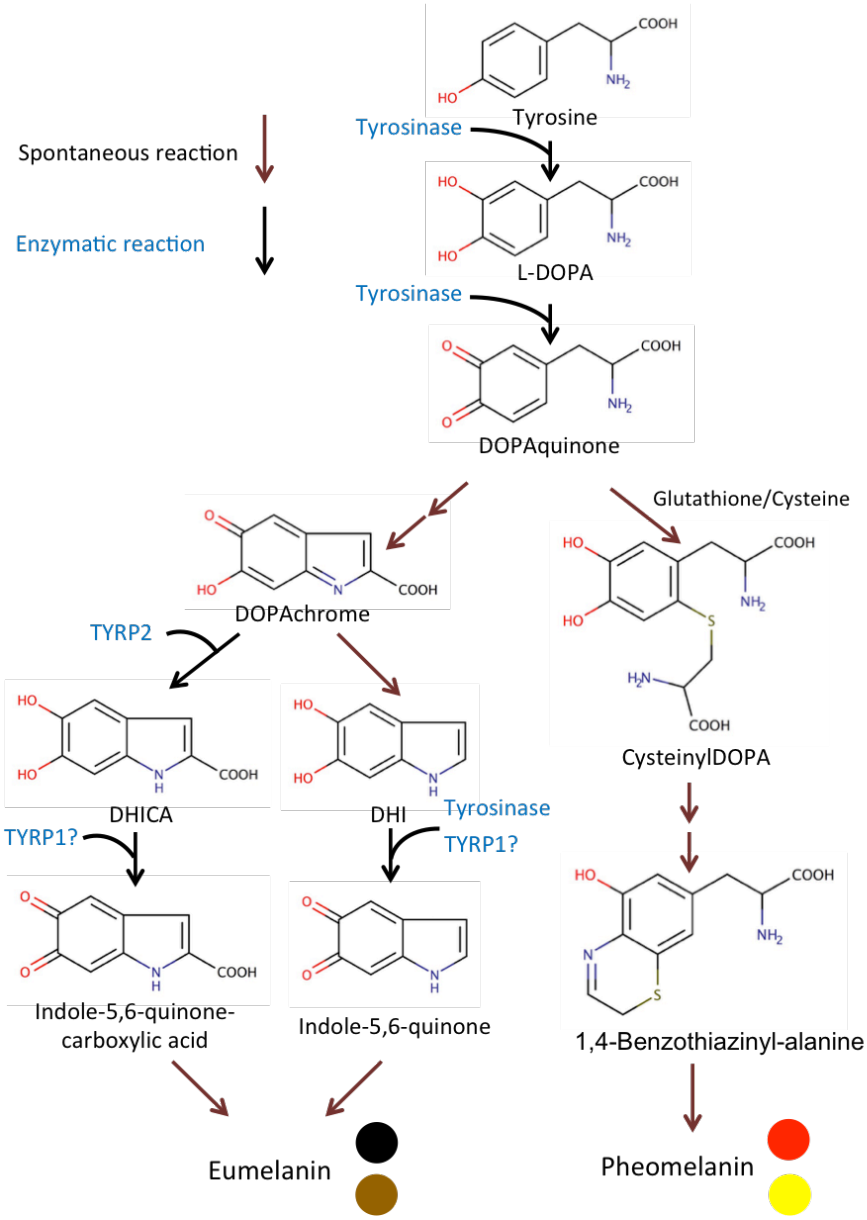

Figure S1. **Melanin biosynthesis pathway.**[18–20] The eumelanin color ranges from black to brown, and that of pheomelanin from yellow to reddish, as indicated by the color filled spheres.

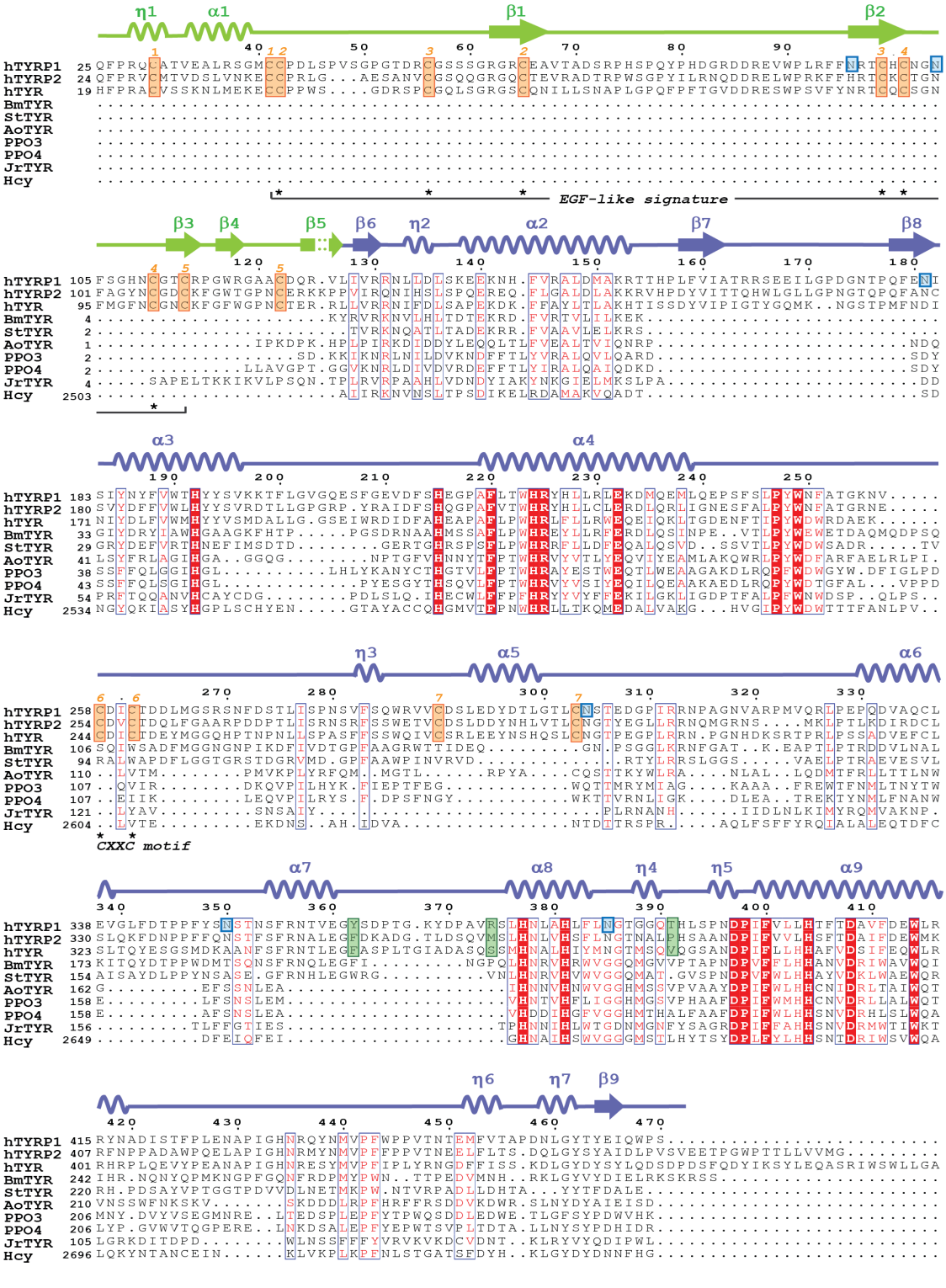

Figure S2. TYRP1 secondary structure and sequence alignment of tyrosinases. Alignment of structurally characterized tyrosinase and tyrosinase-like proteins based on DALI [21] and ClustalW [22]. Human TYRP1, TYRP2 and TYR; mushroom tyrosinases PPO3 (Z-score 21, 17% identity, PDB 2Y9W)[23] and PPO4 (Z-score 20, 20% identity, PDB 4OUA);[24] the closest structural homolog *Bacillus megaterium* tyrosinase (BmTYR, Z-score 33, 33% identity, PDB 3NM8);[6] *Aspergillus oryzae* tyrosinase (AoTYR, Z-score 14, 18% identity, PDB 4J3Q);[25] *Streptomyces* tyrosinase (StTYR, Z-score 29%, 30% identity, PDB 1WX4);[26] walnut tyrosinase (JrTYR, Z-score 21, 19% identity, PDB 5CE9);[27] the oxygen transporter hemocyanin from *Octopus dofleini* (Hcy, Z-score 22, 20% identity,

PDB 1JS8).[28] Residues are numbered according to the TYRP1 amino acid sequence. The TYRP1 secondary structure elements are shown. Disulfide bonds and the involved cysteine residues are indicated in orange numbers. TYRP1 N-glycosylation sites are highlighted in light blue. Non-conserved residues in the active site are highlighted in green. Cys residues conforming to the EGF-like signature pattern [C1-C3, C2-C4, C5-C6] are indicated with an *. The CXXC motif potentially involved in copper incorporation is also indicated.

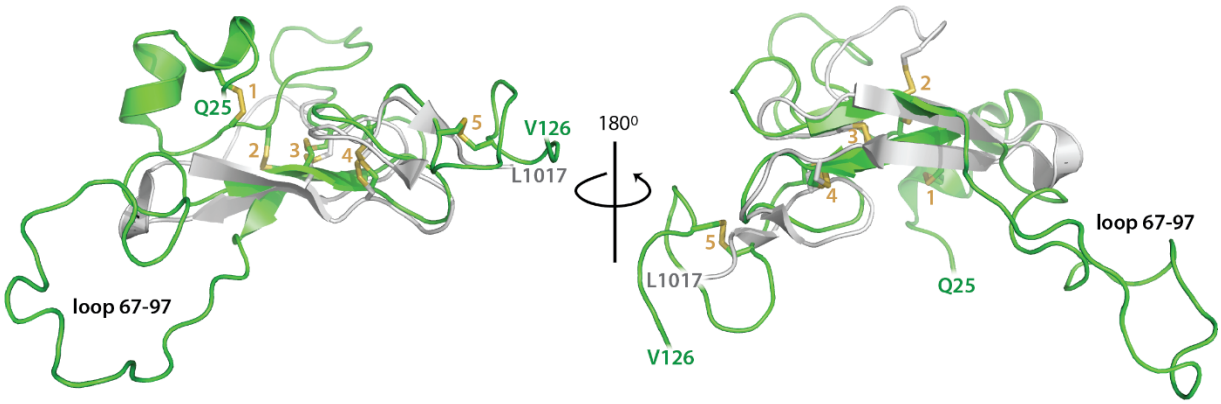

Figure S3. **TYRP1 Cys-rich subdomain folds as an EGF-like domain**. Structural alignment of the TYRP1 Cys-rich subdomain (residues 25-126, green) and the human Epidermal Growth Factor EGF-like domain (976-1017, grey, *PDB 1JL9_A*) based on DALI.[21] Disulfide bonds are shown in yellow sticks and are numbered according to Supplementary Fig. 2.

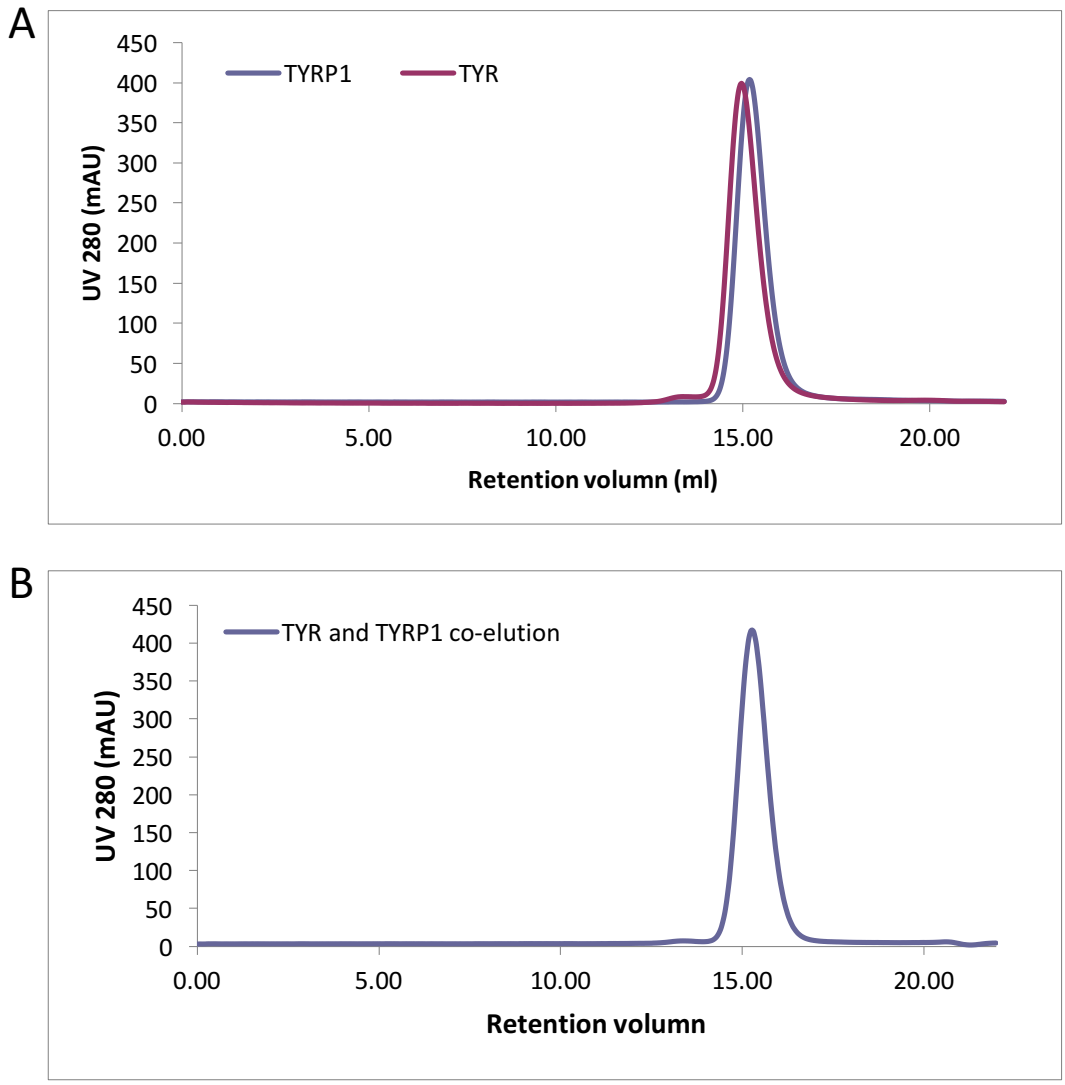

Figure S4. **TYR and TYRP1 are monomeric in solution**. **(A)** Analytical gel filtration profiles of TYR (19-456) and TYRP1 (25-471) overlapped from two individual runs on a Superdex 200 10/300 GL column. **(B)** Analytical gel filtration profile after incubation of a mixture of TYR (19-456) and TYRP1 (25-471) on a Superdex 200 10/300 GL column. Irrespective of being run separately or combined, the samples elute at 15 mL, which corresponds to a MW of around 51 kDa, indicating that the proteins elute as monomeric forms. The buffer used in gel filtration is 20 mM Tris-HCl, pH 7.8, 300 mM NaCl.

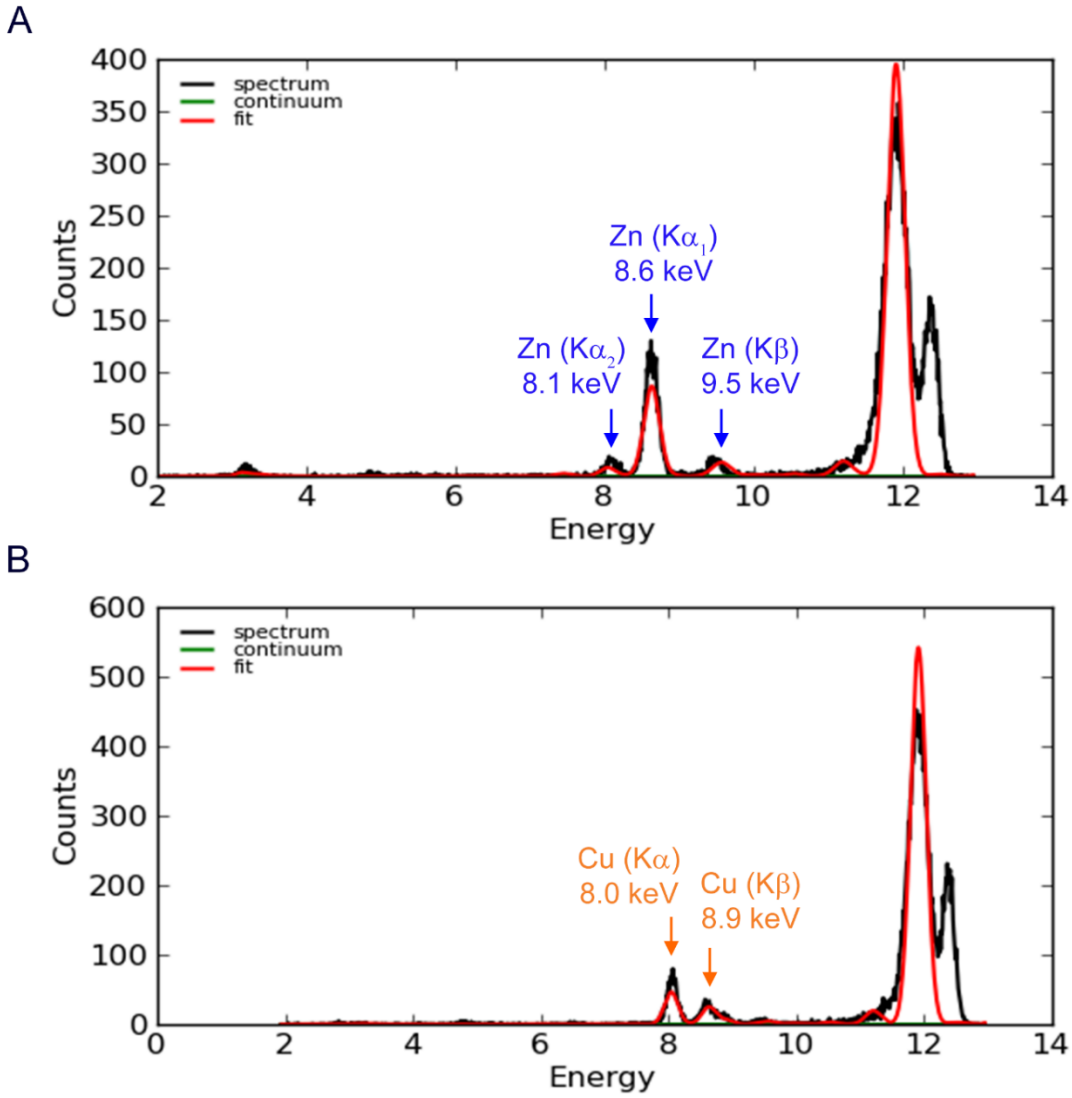

Figure S5. **X-ray fluorescence spectrum of TYRP1 (A) and TYR (B) crystals**. The black line indicates the raw counts (arbitrary scale) on the detector as a function of energy (keV). The red line indicates the fit based on the raw data. The two large peaks on the right of the spectrum are the Compton (inelastic) and the Rayleigh (elastic) scattering peaks of the incident beam. X-ray fluorescence emission energies (κβ and κ*α*) for Zn and Cu are indicated.

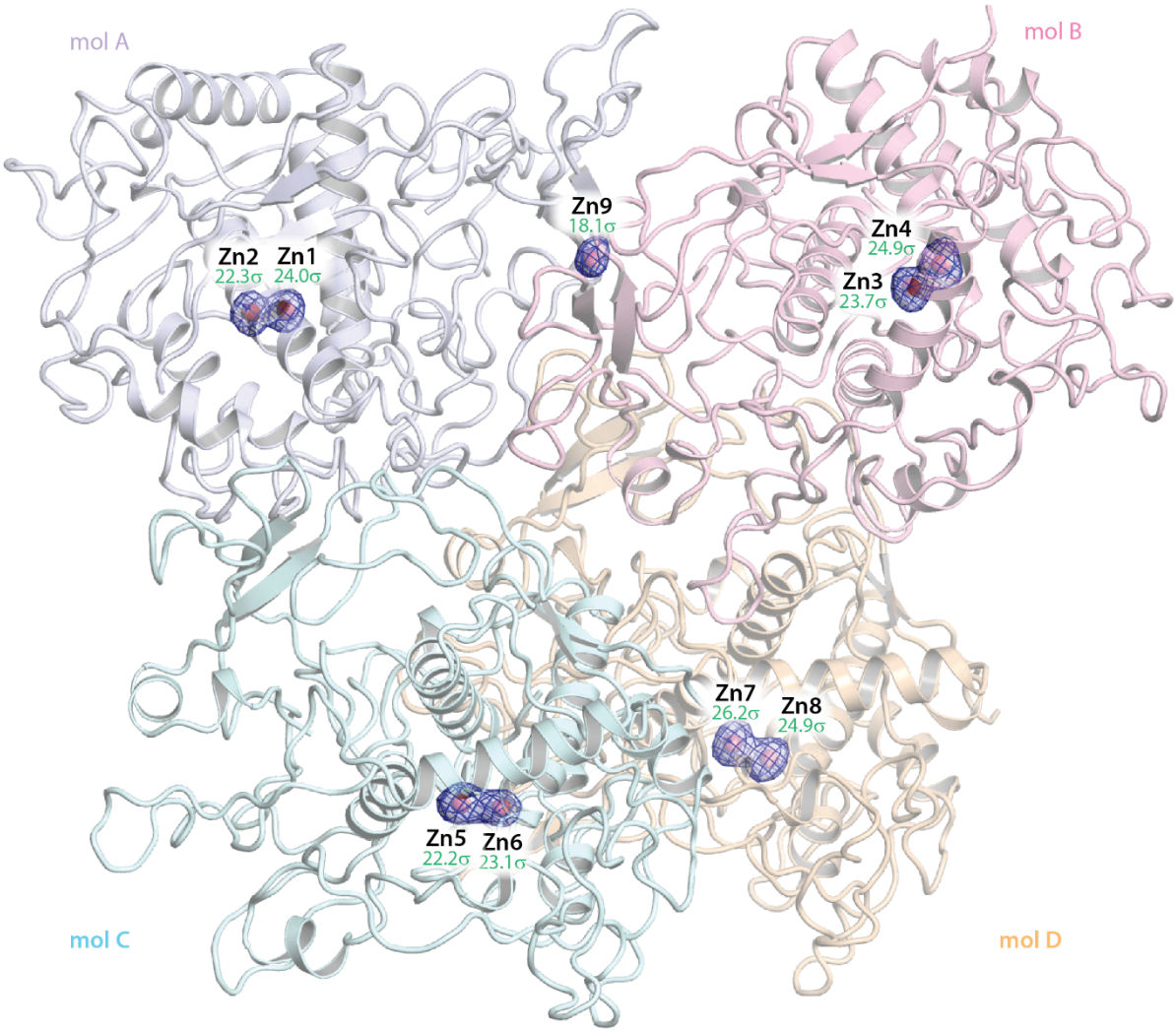

Figure S6. Zinc anomalous difference peaks in the TYRP1 crystal structure. Anomalous difference electron density map from TYRP1 X-ray diffraction data collected at the absorption K-edge of zinc (9.6 KeV) contoured at 3 σ. Nine anomalous difference peaks above 18 σ are present in the asymmetric unit, eight of them in the active sites and an additional one on a non-crystallographic dyad between molecules A and B. The peak heights at the zinc ion positions are indicated. The four molecules A, B, C, and D are displayed in different colors.

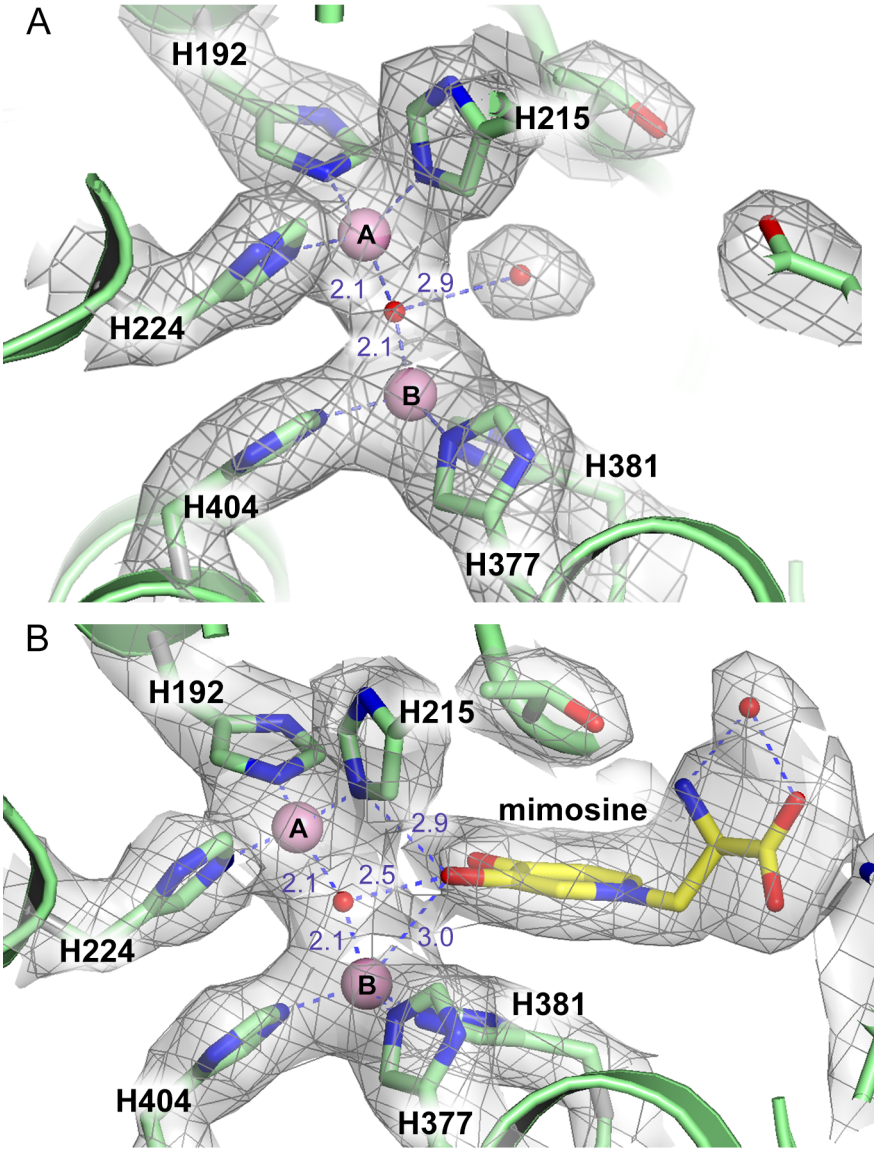

Figure S7. Metal-ion bridging solvent in TYRP1 active site. (A) A close-up of the active site of TYRP1. Zinc-coordinating histidine residues are shown as stick models. The A and B zinc ions are displayed as pink spheres with the water molecules in red. In the absence of substrate, a water molecule makes a hydrogen bond with the metal-ion bridging water. **(B)** In the presence of a substrate analogue like mimosine, the oxygen of a hydroxyl from the substrate makes a hydrogen bond with the oxygen of the metal-bridging water. Metal-solvent coordinating distances are shown as dashed lines and labeled. 2Fo-Fc electron density maps (grey wire) are contoured at 1 σ.

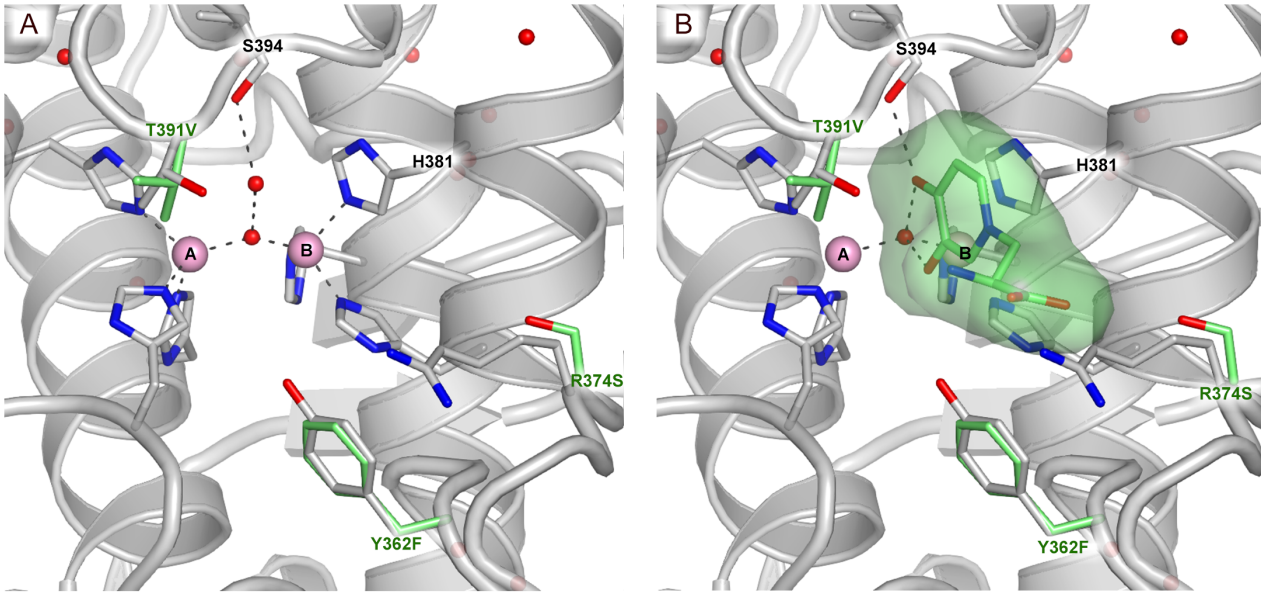

Figure S8. Substrate-binding mode of TYR-mimicked TYRP1 active site. (A) Active site of the TYRP1-3M mutant (Y362F-R374S-T391V), which mimicks the TYR active site, and **(B)** active site of TYRP1-3M with bound mimosine. TYRP1-3M has an identical metal ion coordination to that of native TYRP1. Furthermore, mimosine binds very similarly to native TYRP1, indicating that the stacking interaction of the mimosine aromatic ring with His381 and the water-mediated hydrogen bonds of its aromatic keto- and hydroxyl groups are sufficient for binding. Mutated residues are highlighted in green. Mimosine is shown as green sticks within a green molecular surface.

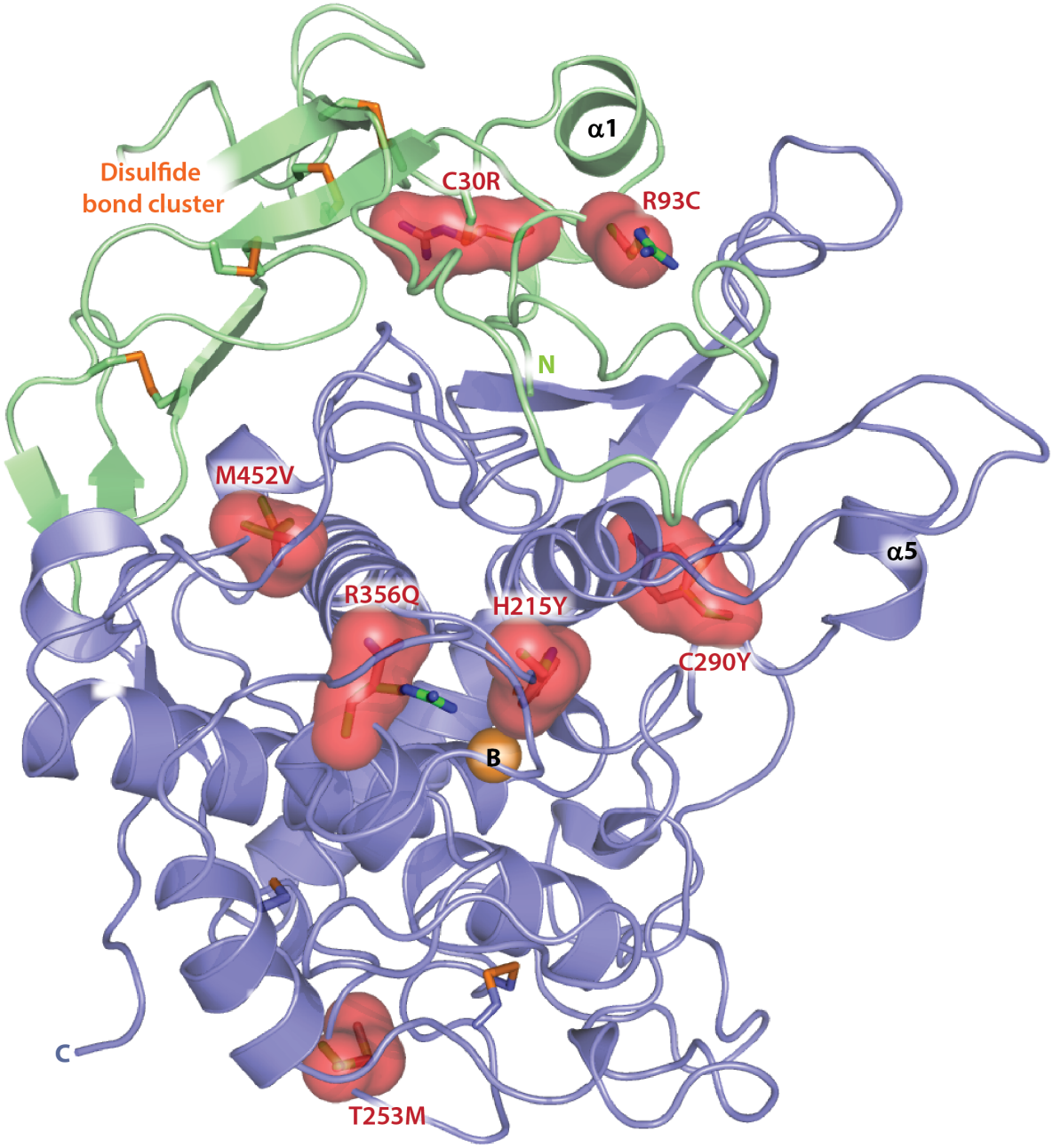

Figure S9. **OCA3 disease and blond hair mutations mapped on the structure of TYRP1.** The Cys-rich subdomain is shown in light green and the tyrosinase-like subdomain in blue. The OCA3-related single-residue mutations are pictured as red sticks surrounded by surfaces. Native residues are shown as green sticks. The blond hair mutation is R93C. The disulfide bond cluster is indicated, and the disulfide bonds are shown as orange sticks. The Zn-B ion is shown as an orange sphere, while the Zn-A ion occupies the same position as the hydroxyl group of the newly introduced tyrosine residue (H215Y). The N and C labels correspond to the N- and C-terminus, respectively.

Supplementary Tables

Supplementary Table 1. Statistics of data collection and refinement for crystal structures of TYRP1.

	Native TYRP1	TYRP1 tyrosine	TYRP1 tropolone	TYRP1 Mimosine	TYRP1 Kojic acid	TYRP1-3M momosine	TYRP1-3M tropolone	TYRP1-3M Kojic acid	Native TYRP1 Zn-edge
Data									
Beamline	ID23-1	ID23-1	ID23-1	ID29	ID29	MASSIF1	MASSIF1	MASSIF1	ID23-1
Wavelength (Å)	0.976	0.976	0.976	0.976	0.976	0.976	0.976	0.976	1.282
Space group	$P2_12_12_1$	$P2_12_12_1$	$P2_12_12_1$	$P2_12_12_1$	$P2_12_12_1$	$P2_12_12_1$	$P2_12_12_1$	$P2_12_12_1$	$P2_12_12_1$
Cell									
a	90.42	89.52	89.69	89.79	90.25,	89.35	89.73	89.64	89.63
b	141.76	140.32	140.20	141.08	141.54	139.73	140.60	140.43	142.29
c	191.74	191.68	191.06	192.26	192.13	190.95	191.25	191.56	192.17
α, β, γ (°)	90, 90, 90	90, 90, 90	90, 90, 90	90, 90, 90	90, 90, 90	90, 90, 90	90, 90, 90	90, 90, 90	90,90,90
Resolution (Å)	48.98-2.35	48.76-2.8	48.69-2.5	48.92-2.6	49.00-2.65	48.60-2.40	48.75-2.35	48.77-2.85	49-3.49
R_{merge} (%)	16.7 (109.4)	12.6 (89.3)	23.1 (85.4)	31.1 (183.7)	14.4 (99.2)	12.4 (89.6)	9.6 (85.1)	18.7 (136.3)	11.5 (38.6)
$I / \sigma I$	6.6 (1.2)	7.6 (1.4)	6.0 (1.7)	5.7 (1.7)	9.0 (1.6)	12.6 (2.1)	11.9 (1.6)	9.9 (1.4)	26.6 (8.3)
Completeness	99.7 (99.8)	99.4 (99.7)	99.8 (99.8)	99.2 (99.8)	99.8 (100)	100 (100)	99.7 (99.2)	100 (100)	100 (99.9)
Redundancy	4.8 (4.9)	3.3 (3.4)	4.8 (4.9)	4.2 (4.4)	4.6 (4.8)	4.8 (7.0)	4.3 (4.0)	6.7 (6.6)	16.4 (15.7)
Anomalous correlation (%)	--	--	--	--	--	--	--	--	26
Refinement									
Resolution (Å)	48.98-2.35	48.76-2.8	48.69-2.5	48.92-2.6	49.00-2.65	48.60-2.40	48.75-2.35	48.77-2.85	
No. reflections	102,816	59,734	83,673	74,895	71,595	94,135	10,0975	57,320	
R_{work} / R_{free}	21.40/25.49	20.46/26.20	20.43/25.12	21.94/27.45	19.67/24.94	20.01/24.86	18.28/22.54	20.79/27.54	
No. of atoms									
Protein	14240	14240	14240	14240	14240	14216	14216	14216	
Water	181	65	179	272	43	39	577	4	
Carbohydrate	696	750	746	617	689	486	678	466	
Zn	9	9	8	9	9	9	8	9	
Ligand		52	36	56	40	56	36	40	
B factors									
Protein	38.946	53.577	24.204	45.102	38.689	38.544	42.728	56.813	
Water	31.365	41.504	20.888	41.274	30.626	30.737	44.080	50.723	
Carbohydrate	59.375	77.788	45.187	61.171	58.645	53.966	60.925	66.491	
Zn	43.727	50.281	26.764	40.713	44.273	29.278	38.359	54.838	
Ligand		62.975	20.319	41.800	44.497	34.788	52.855	59.682	
r. m. s. d.									
Bond lengths	0.011	0.014	0.011	0.012	0.012	0.009	0.011	0.011	
Bond anglee	1.110	1.340	1.140	1.360	1.140	1.130	1.220	1.440	

Supplementary Table 2. Reported activity assays of recombinant human tyrosinase and their experimental conditions.

Reference	Reaction buffer	Reaction temperature	Substrate concentration (L-tyrosine/ L-DOPA)	Additives	Protein construct and expression host	Activity (1/s)
Kong et al., 2010[29]	50 mM Tris-HCl pH7.5	37 °C	Kinetic study	Not specified	Ectodomain (residues 19-474) in E.coli	L-Tyrosine: 36.8 L-DOPA: 33.3
Fogal et al., 2015[30]	100 mM Phosphate pH7.2	Not specified	3mM/5mM	4% DMF and 6.2 mM MBTH	Full-length (SDS was used as solubilizing agent) in insect cells Sf9	L-Tyrosine: 2.37 L-DOPA: 37.3
Dolinska et al., 2014[31]	50 mM Sodium phosphate pH 7.5	37 °C	0.2mM/3mM	For monophenol oxidase activity, 50 uM L-DOPA was added to eliminate lag period	Intra-melanosomal domain in insect larvae Trichoplusia ni	L-Tyrosine: 0.040 L-DOPA: 0.185
This study	125 mM Potassium phosphate pH 6.8	~22 °C	Saturated	2.5% DMF and 5 mM MBTH	Intra-melanosomal domain in insect cells Sf21	L-tyrosine: 0.011 L-DOPA: 0.030

Supplementary References

[1] X. Lai, M. Soler-Lopez, H. J. Wichers, B. W. Dijkstra, *PLoS One* **2016**, Article number e0161697.
[2] M. W. Bowler, D. Nurizzo, R. Barrett, A. Beteva, M. Bodin, H. Caserotto, S. Delagenire, F. Dobias, D. Flot, T. Giraud, et al., *J. Synchrotron Radiat.* **2015**, *22*, 1540–1547.
[3] W. Kabsch, *Acta Crystallogr. Sect. D Biol. Crystallogr.* **2010**, *66*, 125–132.
[4] P. Evans, *Acta Crystallogr. Sect. D Biol. Crystallogr.* **2006**, *62*, 72–82.
[5] M. D. Winn, C. C. Ballard, K. D. Cowtan, E. J. Dodson, P. Emsley, P. R. Evans, R. M. Keegan, E. B. Krissinel, A. G. W. Leslie, A. McCoy, et al., *Acta Crystallogr. Sect. D Biol. Crystallogr.* **2011**, *67*, 235–242.
[6] M. Sendovski, M. Kanteev, V. S. Ben-Yosef, N. Adir, A. Fishman, *J. Mol. Biol.* **2011**, *405*, 227–237.
[7] N. Stein, *J. Appl. Crystallogr.* **2008**, *41*, 641–643.
[8] A. J. McCoy, R. W. Grosse-Kunstleve, P. D. Adams, M. D. Winn, L. C. Storoni, R. J. Read, *J. Appl. Crystallogr.* **2007**, *40*, 658–674.
[9] P. D. Adams, P. V. Afonine, G. Bunkóczi, V. B. Chen, I. W. Davis, N. Echols, J. J. Headd, L. W. Hung, G. J. Kapral, R. W. Grosse-Kunstleve, et al., *Acta Crystallogr. Sect. D Biol. Crystallogr.* **2010**, *66*, 213–221.
[10] P. Emsley, B. Lohkamp, W. G. Scott, K. Cowtan, *Acta Crystallogr. Sect. D Biol. Crystallogr.* **2010**, *66*, 486–501.

[11] G. A. Leonard, V. A. Solé, A. Beteva, J. Gabadinho, M. Guijarro, J. McCarthy, D. Marrocchelli, D. Nurizzo, S. McSweeney, C. Mueller-Dieckmann, *J. Appl. Crystallogr.* **2009**, *42*, 333–335.
[12] V. A. Solé, E. Papillon, M. Cotte, P. Walter, J. Susini, *Spectrochim. Acta - Part B At. Spectrosc.* **2007**, *62*, 63–68.
[13] J. Gabadinho, A. Beteva, M. Guijarro, V. Rey-Bakaikoa, D. Spruce, M. W. Bowler, S. Brockhauser, D. Flot, E. J. Gordon, D. R. Hall, et al., *J. Synchrotron Radiat.* **2010**, *17*, 700–707.
[14] A. J. Winder, H. Harris, *Eur. J. Biochem.* **1991**, *198*, 317–326.
[15] J. C. Espín, M. Morales, P. A. García-Ruiz, J. Tudela, F. García-Cánovas, *J. Agric. Food Chem.* **1997**, *45*, 1084–1090.
[16] T. Kobayashi, K. Urabe, A. Winder, C. Jiménez-Cervantes, G. Imokawa, T. Brewington, F. Solano, J. C. García-Borrón, V. J. Hearing, *EMBO J.* **1994**, *13*, 5818–5825.
[17] M. Martinez-Esparza, C. Jimenez-Cervantes, J. C. Garcia-Borron, J. A. Lozano, V. del Marmol, G. Ghanem, F. Solano, *Pigment Cell Res* **1997**, *10*, 229–235.
[18] V. J. Hearing, K. Tsukamoto, *FASEB J.* **1991**, *5*, 2902–2909.
[19] P. Aroca, K. Urabe, T. Kobayashi, K. Tsukamoto, V. J. Hearing, *J. Biol. Chem.* **1993**, *268*, 25650–25655.
[20] A. Slominski, D. J. Tobin, S. Shibahara, J. Wortsman, *Physiol. Rev.* **2004**, *84*, 1155–1228.
[21] L. Holm, P. Rosenström, *Nucleic Acids Res.* **2010**, *38*, DOI 10.1093/nar/gkq366.
[22] M. A. Larkin, G. Blackshields, N. P. Brown, R. Chenna, P. A. Mcgettigan, H. McWilliam, F. Valentin, I. M. Wallace, A. Wilm, R. Lopez, et al., *Bioinformatics* **2007**, *23*, 2947–2948.
[23] W. T. Ismaya, H. J. Rozeboom, A. Weijn, J. J. Mes, F. Fusetti, H. J. Wichers, B. W. Dijkstra, *Biochemistry* **2011**, *50*, 5477–5486.
[24] S. G. Mauracher, C. Molitor, R. Al-Oweini, U. Kortz, A. Rompel, *Acta Crystallogr. D. Biol. Crystallogr.* **2014**, *70*, 2301–2315.
[25] N. Hakulinen, C. Gasparetti, H. Kaljunen, K. Kruus, J. Rouvinen, *J. Biol. Inorg. Chem.* **2013**, *18*, 917–929.
[26] Y. Matoba, T. Kumagai, A. Yamamoto, H. Yoshitsu, M. Sugiyama, *J. Biol. Chem.* **2006**, *281*, 8981–8990.
[27] A. Bijelic, M. Pretzler, C. Molitor, F. Zekiri, A. Rompel, *Angew. Chemie - Int. Ed.* **2015**, *54*, 14677–14680.
[28] M. E. Cuff, K. I. Miller, K. E. van Holde, W. A. Hendrickson, *J. Mol. Biol.* **1998**, *278*, 855–870.
[29] J.-N. Kong, H.-J. Lee, D.-H. Jo, K.-H. Kong, *Protein Pept. Lett.* **2010**, *17*, 1026–1030.
[30] S. Fogal, M. Carotti, L. Giaretta, F. Lanciai, L. Nogara, L. Bubacco, E. Bergantino, *Mol. Biotechnol.* **2015**, *57*, 45–57.
[31] M. B. Dolinska, E. Kovaleva, P. Backlund, P. T. Wingfield, B. P. Brooks, Y. V Sergeev, *PLoS One* **2014**, *9*, e84494.